Journal of Luminescence 206 (2019) 292–297

Contents lists available at ScienceDirect

Journal of Luminescence

journal homepage: www.elsevier.com/locate/jlumin

Nanostructured ZnS:Cu phosphor: Correlation between photoluminescence properties and local structure

Ana Laura Curcio[a,b], Luís Fernando da Silva[b], Maria Inês Basso Bernardi[c], Elson Longo[d], Alexandre Mesquita[a,*]

[a] Institute of Geosciences and Exact Sciences, São Paulo State University, Unesp, Rio Claro, SP, Brazil
[b] Department of Physics, Federal University of São Carlos, UFSCar, São Carlos, SP, Brazil
[c] São Carlos Institute of Physics, University of São Paulo, USP, São Carlos, SP, Brazil
[d] LIEC, Department of Chemistry, Federal University of São Carlos, UFSCar, São Carlos, SP, Brazil

ABSTRACT

Zinc sulfide (ZnS) is a II–VI inorganic semiconductor material and has received remarkable attention because of fundamental physical properties, versatility, nontoxicity, chemical stability and has been widely applied to make numerous optical devices as phosphor material. As a wide band gap semiconductor, ZnS can easily host different metal ions as luminescent center to improve or modify its structural and optical performances such as Cu atoms. In this paper, ZnS:Cu nanoparticles were synthesized by solvothermal method and the photoluminescence and the structural at long- and local-range properties were characterized. According to X-ray diffraction results, ZnS sample crystallizes with the cubic zinc blende structure (*F*-43*m* space group) without spurious phases. Images from transmission electron microscope depict the morphology of ZnS particles as round shape and average size value lower than 5 nm. Theoretical and experimental X-ray absorption near edge structure (XANES) spectra at Zn K-edge suggest the incorporation of Cu atoms into the ZnS host and indicate the occurrence of Zn and S vacancies, which are confirmed by extended X-ray absorption fine structure (EXAFS) fit results. These native defects are related to a red-shift observed in the peak emission of photoluminescence (PL) spectrum for ZnS sample, which is centered at ~ 504 nm. An emission in orange-red region is observed as Cu is incorporated in the ZnS host matrix that is attributed to the transition from the $^4T_1$ level to the $^6A_1$ level. Moreover, the intensity of the emissions due to zinc vacancies and interstitial zinc in the deconvoluted PL spectrum is in accordance with results determined in X-ray absorption spectroscopy characterization.

1. Introduction

II-VI group inorganic semiconductor such as ZnO, SnO_2, TiO_2, CdS,CdSe, ZnSe, and ZnTe are well-known because of their interesting luminescence, magnetic, and electrical properties [1–6]. Zinc sulfide (ZnS) is also a II–VI inorganic semiconductor material and has received remarkable attention because of fundamental physical properties, versatility, non-toxicity, chemical stability and potential for several technological applications [1,3,4,6]. Due to its wide band gap with a range of energy of 3.7–3.9 eV and high exciton binding energy (40 meV), ZnS has been widely applied innumerous optical devices such as ultraviolet light-emitting diodes, flat panel display, lasers, photodectors, phosphor in electroluminescent devices and solar cells [1,3,4,6]. Furthermore, the ZnS compound also exhibits activity in photodegradation of organic materials due to trapped holes arising from surface defects on the sulfide.

Considering its wide band-gap semiconductor behavior, ZnS can easily host different metal ions as luminescent center to improve or modify its structural and optical performances [3,5]. Incorporation of dopants/impurities produces discrete energy levels in the intrinsic quantum energy levels, which in turn enhances the optical, electronic, and magnetic properties of the host semiconductor. Different metal ions, such as Mn^{2+}, Cu^{2+}, Pb^{2+}, Ag^{+}, Cr^{3+}, $Ni^{2+}$and Eu^{2+}, have been successfully incorporated into ZnS lattice [4–7]. The doping process has as main purpose to modulate its luminescence properties by forming of the various energy levels within the band gap of the host.

Photoluminescence properties of ZnS compound can also be tuned with the variation of crystallite size. It is well-established when tiny particles have high surface/volume ratio and surface atoms, and consequently few neighboring coordinate atoms, which can be treated as defects [5,7]. These defects contribute to the presence of further electronic states in the band gap, which can mingle with the intrinsic states to a substantial extent and affect the spacing of the energy levels and the optical properties of nanoparticles. Thus, the reduction of particle size changes the band structure of the semiconductor, increasing the band gap and the edges of the band split into discrete energy levels [1,5]. These effects have attracted the attention in research of nanocrystalline ZnS. This inorganic compound is a multifunctional material that presents a variety of crystal shapes, such as rods, belts, cages, combs, rings and helixes [1,4]. These ZnS nanostructures with

* Corresponding author.
E-mail address: mesquita@rc.unesp.br (A. Mesquita).

https://doi.org/10.1016/j.jlumin.2018.10.073
Received 25 May 2018; Received in revised form 11 September 2018; Accepted 15 October 2018
Available online 16 October 2018

controllable crystal phase and shape are highly desirable for exploiting novel properties and extending their applications. To achieve this goal, several techniques have been employed to synthesize ZnS nanoparticles, such as precipitation, sol–gel, solvothermal and thermal coevaporation at high temperature [3,6,7]. Among these routes, the solvothermal method requires a relatively low temperature, cheap precursors with low toxicity besides facilitating the introduction of transition metal ions such as copper into the ZnS lattice [3].

In order to interpret photoluminescence properties of the nanocrystalline ZnS, structural characterizations become useful to gain insight into the correlation between optical and structural properties by mean of the associated energy levels [8]. The site-selective structural technique is the X-ray absorption spectroscopy (XAS) is a powerful tool to investigate the local structure, proving meaningful further structural information [9]. It is important to note that, despite the local structural data afforded by XAS are usually not sufficient to construct a whole structural model, they often provide valuable information about the local structural peculiarities [10].

In this manuscript, we investigated the influence of Cu doping in the properties of ZnS nanoparticles synthesized via solvothermal method. To attain this objective, we applied a variety of characterization techniques, which include X-ray diffraction (XRD), high-resolution transmission electron microscopy (HR-TEM), X-ray absorption spectroscopy (XANES and EXAFS regions) and photoluminescence spectroscopy. The focus of this investigation is to provide an understating of the effect of Cu addition on the structural (long- and short-range order) and optical properties of nanostructured ZnS compound.

2. Experimental procedure

The $Zn_{1-x}Cu_xS$ samples (x = 0.00% and 1% mol – labeled as ZnS and ZnS: Cu, respectively) were prepared via solvothermal method. This route is based on chemical co-precipitation method at room temperature. This metodology presents some advantages over other preparation techniques, which include the stoichiometry control, purity and homogeneity of the as-obtained particles [3]. Zinc dichloride ($ZnCl_2$– Aldrich, 98%), copper nitrate trihydrate ($Cu(NiO_3)_2{\cdot}3H_2O$– Aldrich, 98%) and thiourea (H_2NCSNH_2– Aldrich 99%) were used as reagents, which were diluted in ethylene glycol ($C_2H_6O_2$– Synth 99,5%). Afterwards, a sodium hydroxide solution (NaOH–Vetec, 97%) was dropped and then placed in a sealed 110 mL Teflon autoclave. The precursor solutions were heated-treated by conducting heat under constant stirring at 140 °C during 30 min with a rate of 10 °C/min. After the treatment, the autoclave was naturally cooled to room temperature. At the end, the precipitated powders were washed several times with deionized water until a neutral pH was attained, and then the powder samples were dried at 80 °C for 12 h.

Room-temperature X-ray diffraction (XRD) measurements were performed in a RigakuUltima 4 powder diffractometer with geometry θ–2θ, with a rotating anode X-ray source (Cu-Kα radiation, λ = 1.542 Å), and a scintillation detector. The data were collected with a 0.02° step size at a 5 s per step. High-resolution transmission electron microscopy (HR-TEM) images were performed using a FEI microscope (TECNAI G2T F20) operating at 200 kV. The energy dispersive X-ray analysis (EDX) was performed in a scanning electron microscope (SEM, FEI-Philips, model XL30-FEG), with resolution of 2 nm operating at 30 kV coupled with a spectrometer EDAX-AMETEC (model APPOLLO X).

Zn K-edge X-ray absorption spectra (9659 eV) were collected at the LNLS (Brazilian Synchrotron Light Laboratory) facility using the D04B-XAS1beamline. The LNLS storage ring was operated at 1.36 GeV and 100–160 mA. These spectra were collected in transmission mode using an Si(111) channel-cut monochromatorat room temperature. The samples thicknesses were optimized at each edge by the Multi-Platform Applications for XAFS (MAX) software package Absorbix code [11]. Normalized XANES and EXAFS spectra were extracted with the MAX-Cherokee code while the fitting procedure and comparison between experimental and theoretical EXAFS curves were conducted with the MAX-Roundmidnight package. The theoretical EXAFS spectra were calculated by the FEFF9ab initio code [12] whose input files were issued from MAX-Crystalffrev software, which takes in account substitution disorder and random vacancies in the structure. In our work the relevant measure of the fit quality, the reduced statistical $\chi 2$, is named QF (quality factor).

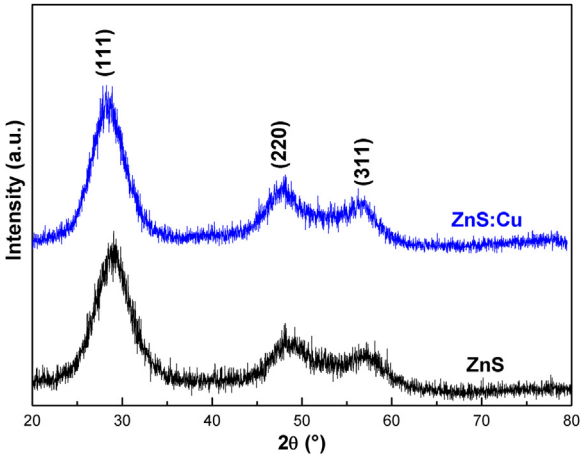

Fig. 1. XRD patterns of ZnS and ZnS:Cu samples.

Room-temperature photoluminescence spectra were collected with a Thermal Jarrel-Ash Monospecmonochromator and a Hamamatsu R446 photomultiplier. The 350.7 nm exciting wavelength of a krypton ion laser (Coherent Innova) was used; the output of the laser was maintained at 200 mW.

3. Results and discussion

Fig. 1 shows the XRD patterns of theas-prepared ZnS and ZnS:Cu samples. The samples presented diffraction planes of the samples correspond to the cubic zinc blende (sphalerite) structure with *F*-43*m* space group [13]. It should be noted that presence of spurious phases was not observed within the investigated detection limit. Furthermore, it is observed significant broadening of the diffraction peaks which is ascribed of smaller crystallite size. The average crystallite size was calculated, by Scherrer equation, [14] using the full width at half maximum of (111) peaks from the XRD patterns for the samples depicted in Fig. 1. The obtained values are of approximately 2 nm, comparable to ZnS compound prepared by the same methodology reported in a previous work [15].

The TEM and HRTEM images of the ZnS:Cu samples are displayed in Fig. 2, respectively. From the analysis of Fig. 2(a), it can be observed that ZnS:Cu sample presented a non homogeneous size distribution and necked particles, showing a quasi-spherical shape. Additionally, the particle size ranged between 4 and 10 nm, according to the measure of approximately 100 particles. Furthermore, from the analysis of HRTEM image, Fig. 2(b), it is possible to determine the distance of between neighboring planes is approximately 0.313 nm, which is consistent with the (111) plane in the cubic zinc blende structure of ZnS, in good accordance with XRD data. The EDS spectrum confirmed Zn, S, and Cu elements in the ZnS:Cu sample, as displayed in Fig. 2(c).

An EXAFS study was conducted at the Zn K-edge for more quantitative structural information about the Zn local order. Fig. 3 shows the fitted back Fourier transformed EXAFS spectra and k^3 weighted Fourier transforms of the ZnS standard and nanostructured samples. Fourier transform curves were then back Fourier transformed between 1.0 and 5.0 Å to obtain the experimental EXAFS spectra to fit using a theoretical model calculated from FEFF9 code [12] and CRYSTALFREV [11] software with crystallographic information according to XRD data. The first

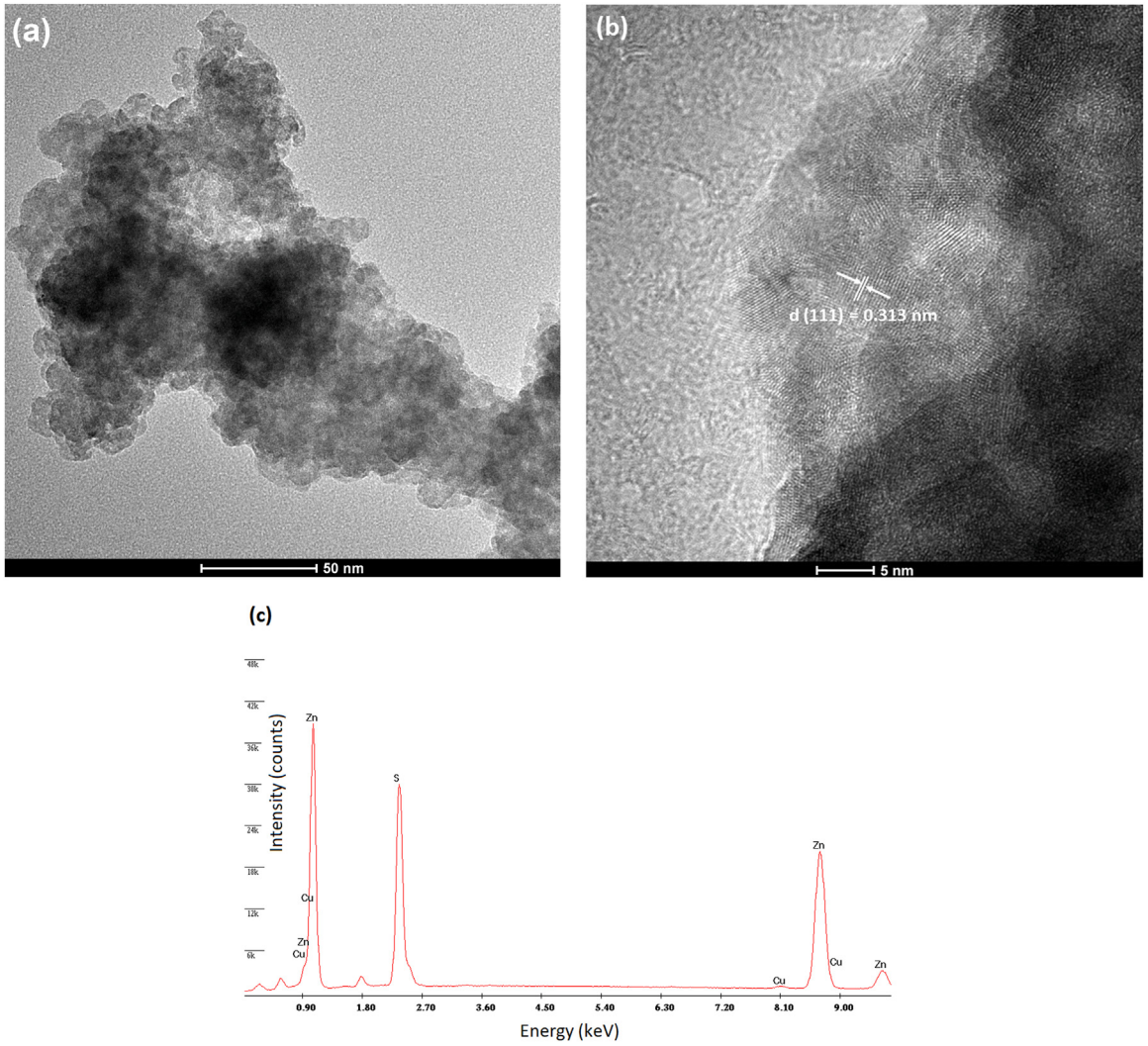

Fig. 2. TEM images for ZnS sample. Fig. 2(b) is a higher-magnified detail of Fig. 2(a). Fig. 2(c) shows EDS spectrum confirming Zn, S, and Cu elements in the ZnS:Cu sample.

intense FT peak is related to the Zn-S distances on the Zn-S tetrahedral site, whereas the peaks beyond the first neighbors (R > 2.5 Å) represent single scattering paths relative to Zn-Zn and Zn-S and multiple scattering paths, such as Zn-S-S, Zn-S-Zn-S, Zn-S-S-S and Zn-Zn-S interactions.

Initially, the EXAFS spectra were fitted according to a local cubic symmetry model based on the XRD results with different sets (coordination shells) of Zn-S and Zn-Zn mean bond-lengths. Each shell can be represented by four fitted parameters, namely number of neighbors (N), Debye-Waller factor (DW), representing the local disorder (σ^2), central atom-neighbor distance (R) and shift of the energy origin ΔE_0.

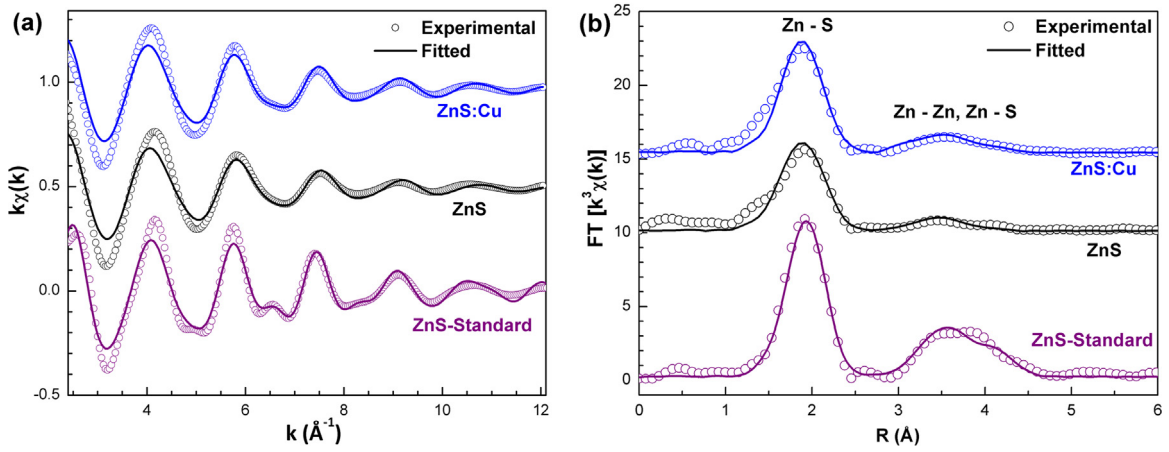

Fig. 3. Fitted and experimental (a) back Fourier transformed EXAFS spectra and (b)k^3-weighted Fourier transforms of the ZnS:Cu samples.

Table 1
EXAFS simulation results of Zn K-edge spectra. R is the distance from the central atom, N is the average coordination number, σ^2 the Debye-Waller factor and QF the quality factor.

Sample	Shell	R (Å)	N	σ^2 (Å^2)	QF
ZnS standard	Zn-S_I	2.33(1)	4.2(8)	0.0027(19)	
	Zn-Zn_I	3.83(2)	10.2(1.2)	0.0144(27)	1.52
	Zn-S_{II}	4.48(1)	7.7(1.4)	0.0027(19)	
ZnS	Zn-S_I	2.30(1)	3.8(5)	0.0067(18)	
	Zn-Zn_I	3.77(2)	6.1(2.1)	0.0202(47)	1.41
	Zn-S_{II}	4.42(1)	0.6(1.3)	0.0067(18)	
ZnS:Cu	Zn-S_I	2.32(1)	4.2(4)	0.0062(17)	
	Zn-Zn_I	3.77(1)	4.6(2.3)	0.0180(29)	2.33
	Zn-S_{II}	4.38(1)	0.4(1.1)	0.0060(12)	

However, the number of parameters (N_{par}) must be minimized for the avoidance of fitting drawbacks due to the poor statistics of the data (on the parameters correlations). The number of free parameters was kept smaller than the number of independent points, which is defined as $N_{ind} = 2\Delta R\Delta k/\pi$, where ΔR is the width of the R-space filter windows and Δk is the actual interval of the fit in the k-space [16]. Therefore, the Debye Waller factor was considered the same for same shells. The energy threshold ΔE_0 adjustment was also constrained to a unique value, since the use of different energies may lead to unphysical results. Table 1 shows the best fitting results for each sample defined by the minimum value of QF. As seen in Table 1, the obtained QF factors indicate the reliability of the fits, which is confirmed by the comparison of the fitted (lines) and experimental (symbols) data presented in Fig. 3.

In our previous study concerning Mn-doped nanostructured ZnS samples and EXFAFS analysis [17], no alterations within the uncertainty are observed in the distance between each shell and Zn absorber atom. On the other hand, Debye-Waller factor values exhibited larger values for samples synthesized via solvothermal route, which would be expected for nanostructured materials. Furthermore, the average coordination number decreased considerably for nanostructured samples in second and third shells. Thus, the fits of EXAFS spectra indicate a significantly number of vacancies in both S and Zn sites for ZnS nanoparticles, which suggest the presence of imperfectness in the crystal lattice. As can be seen in Table 1, similar results are observed in the Cu-doped samples. As the average crystallite size is lower than 5 nm, previously confirmed by TEM analyses, a large amount of the atoms should be placed at the boundary of particles resulting in a lower number of neighbors [18]. Moreover, it was also observed a reduction in the average coordination number of Zn-Zn shell with the Cu incorporation.

We also analyzed the XANES spectra of the XAS measurements in order to obtain more information concerning the local structure of ZnS:Cu samples. XANES spectra give information on the coordination symmetry and the valence of ions incorporated in a solid. The energy of the absorption edge shifts according to the valence of the absorbing ion, since the binding energy of bound electrons rises as the valence increases. Also, the shape of the absorption edge depends on the unfilled local density of states and the coordination symmetry of the absorbing element. The spectrum at the Zn K-edge is characteristic of the electron transition from the 1s state to empty 4p states. In our previous study [17], we performed successfully ab initio calculations which allowed the achievement of theoretical XANES spectra at Zn K-edge. As a result of the comparison between theoretical and experimental XANES spectra, we could understand the shape of the spectra in terms of nanoscaled ZnS particles and concluded that Mn ions are actually incorporated in Zn sites of sphalerite structure [17]. In order to achieve information concerning Cu incorporation and some features of the XANES spectra, we applied this characterization for the ZnS:Cu samples.

Fig. 4 exhibits XANES spectrum at Zn K-edge of the microcrystalline

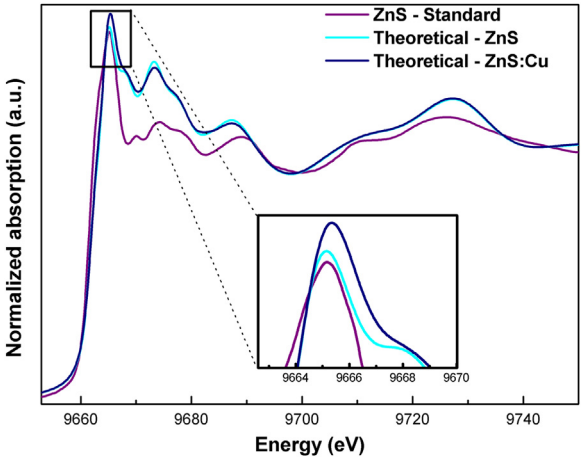

Fig. 4. Experimental XANES spectra of ZnS standard and theoretical XANES spectra for pure ZnS and ZnS:Cu sample. The lower-right inset shows details of white line of these spectra.

ZnS standard compound, which shows similar K-edge white line shapes and XANES features to those previously reported for tetrahedral coordinated ZnS [17,19–21]. Calculated XANES spectrum for ZnS (light blue line) compound using ab initio FEFF code [12] is also shown in this Fig., whose details of calculation can be found elsewhere [17]. As can be observed, the calculated XANES spectra reproduce satisfactorily the experimental spectra. In order to investigate the influence of Cu-doping on the XANES spectra, Cu atoms were randomly incorporated at Zn sites of ZnS structure and the calculated XANES spectra are also shown (dark blue line). As it can be seen in the inset of Fig. 4, the intensity of white line increases as Zn atoms are substituted by Cu atoms. This increase can be related to the fact that the K-edge XANES here reproduces the density distribution of the unoccupied p-like states around Zn atoms. Reduction of the Zn atomic content causes an increased localization of the Zn p-like states and, in consequence, sharper resonances [20].

Fig. 5 shows the normalized Zn K-edge XANES spectra of ZnS standard, ZnS and nanostructured ZnS:Cu samples. The upper-left inset shows the only difference between the spectra of nanostructured ZnS and ZnS:Cu samples: the intensity of white-line peak is higher for ZnS:Cu than ZnS sample. This result is in good accordance with the calculated XANES spectra shown in Fig. 4, indicating undoubtedly that Cu atom are incorporated at Zn sites in ZnS structure. In our previous study, we also observe an increase of the white line at Zn K-edge spectra of ZnS samples with Mn-doping, although a lower increase compared to

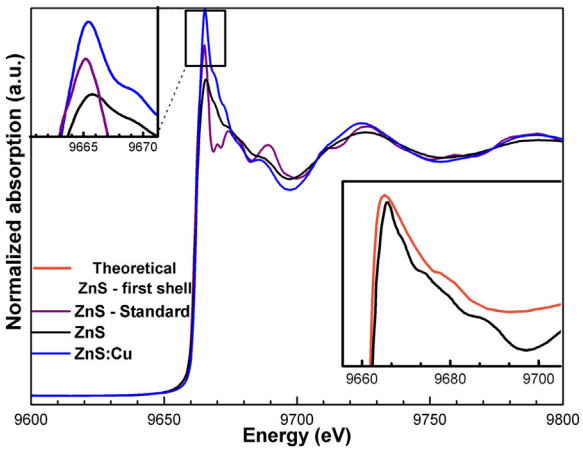

Fig. 5. XANES spectra for ZnS:Cu samples. The upper-left inset shows details of white line and the lower-right inset shows theoretical XANES calculated with one shell of S neighbors around Zn absorber atom.

the spectrum of ZnS:Cu sample [17]. This result indicates an increased of unoccupied *p*-like states around Zn atoms due to defects caused by Cu incorporation.

On the other hand, the XANES spectra of nanostructured samples are considerable different to the spectrum of ZnS standard. The intensity of white line is lower and all the features in XANES region are less discernible. In order to assess these characteristics, theoretical XANES spectrum was obtained considering in the calculation only the first shell of four S atoms around absorber Zn atom. The lower-right inset in Fig. 5 shows this spectrum compared to the XANES spectrum of nanostructured ZnS and, as can be observed, this theoretical spectrum agrees well with the experimental one. Although the main features of the Zn K-edge structure (i.e., the three peaks between 9660 and 9700 eV) are well reproduced with the atoms of the first coordination sphere [21], the XANES spectrum calculated suppressing the second shell with 12 Zn atoms shows good agreement to experimental spectra. This theoretical XANES spectrum considered only the first shell around Zn atoms to generate all the features. Note that the spectrum is in good agreement with fit results of the EXAFS spectra, where S coordination number decreases for nanostructured samples.

Fig. 6 shows the photoluminescence (PL) spectra for pristine ZnS and ZnS:Cu, respectively. As it can be seen, the spectrum of the pristine sample is highly asymmetrical, broadened and centered at approximately 504 nm, exhibiting various peaks which indicates the involvement of different luminescence centers in the radiative processes. This spectrum exhibits similar features compared to that one reported by Ferrer et al. [15], although reports from different groups have shown PL spectra of ZnS compound centered at lower wavelengths.

It has been reported that ZnS compound presents four blue-green emissions located at 417, 446, 480 and 520 nm which arise due to interstitial S lattice defects ($_{Si}$), interstitial Zn lattice defects (Zn_i), S vacancies (V_S) and Zn vacancies (V_{Zn}), respectively [22]. Thus, as shown in Fig. 6(a), Gaussian curve fitting was applied to deconvolute the PL curve for ZnS sample, considering four radiative processes at 2.14, 2.41, 2.66 and 2.89 eV. Since S ions have larger ionic radii (1.7 Å) than that of Zn ions (0.74 Å), interstitial S produces more strain in the ZnS lattice and thus the electron levels due to this site will have smaller binding energy [22]. Therefore, interstitial S energy levels must be closer to valence band than the interstitial Zn energy levels to the conduction band. Similarly S vacancy states are closer to conduction band edge than Zn vacancies states to the valence band edge [22]. Thus, the red-shift observed in Fig. 6(a) for nanostructured ZnS sample could be related to the presence of S and Zn vacancies, as previously evidenced by XAS analyses.

Fig. 6(b) shows the PL spectrum for ZnS:Cu sample. From the analysis of the spectrum, it was identified emissions in blue-yellow region

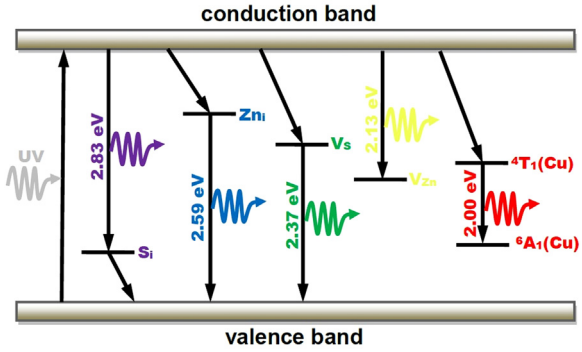

Fig. 7. Schematic diagram of the various emissions corresponding to PL spectrum for ZnS:Cu sample.

for ZnS sample, beyond a shoulder in orange-red region. Several studies devoted to Cu-doped ZnS crystals have reported the blue, green, and orange-red light emissions [4,23,24]. It is reported that Cu incorporation in Zn sites in ZnS crystals introduces a trap energy level, where electron and hole can be trapped. An electron can undergo photo-excitation process in the host ZnS lattice and consequently decay via transition from the $^4T_1$ level to the $^6A_1$ level [4,25]. Thus, this emission could be attributed to the radiative decay between those localized states of Cu inside the ZnS band-gap [4]. The Gaussian deconvolution in Fig. 6(b) shows that this emission is centered at 2.00 eV, whereas the position of other four peaks do not exhibit substantial difference compared to ZnS sample. The only observed difference is the intensity of the peaks that are attributed to the emissions due to V_{Zn} (increase) and Zn_i (decrease) with Cu incorporation. A schematic diagram of the various emissions corresponding to PL spectrum for ZnS:Cu sample is shown in Fig. 7. Based on the XAS analyses, in fact, the S coordination number does not present modification for ZnS:Cu compared to ZnS sample, whereas decrease in Zn coordination number is detected, in agreement, therefore, with these PL results.

4. Conclusions

In summary, ZnS:Cu nanoparticles were synthesized by solvothermal method and the photoluminescence and the structural at long- and local-range properties were characterized. According to XRD results, ZnS sample crystallizes with the cubic zinc blende structure (*F*-43*m* space group) without spurious phases. The TEM images depict morphology of ZnS particles as round shape and average size value lower than 5 nm. Theoretical and experimental XANES spectra at Zn K-edge suggest the incorporation of Cu atoms into the ZnS host and

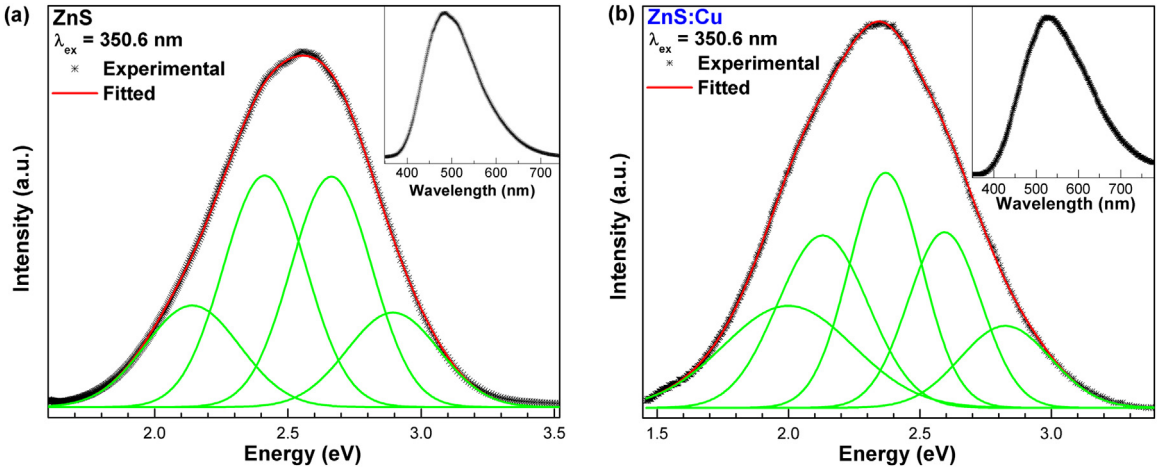

Fig. 6. Photoluminescence for (a) ZnS and (b) ZnS:Cu samples.

indicate the occurrence of Zn and S vacancies, which are confirmed by EXAFS fit results. These native defects are related to a red-shift observed in the peak emission of photoluminescence spectrum for ZnS sample, which is centered at approximately 504 nm. An emission in orange-red region is observed as Cu is incorporated in the ZnS host matrix that is attributed to the transition from the $^4T_1$ level to the $^6A_1$ level. Moreover, the intensity of the emissions due to zinc vacancies and interstitial zinc in the deconvoluted PL spectrum is in accordance with results determined in XAS characterization.

Acknowledgements

The authors thank FAPESP (through projects 2013/12993-4, 2017/12437-5 and 2013/07296-2) and CNPq (473568/2013-6) funding agencies. The authors also thank Mr. Rorivaldo Camargo for the TEM analyses. This research was partially carried out at LNLS National Laboratory of Synchrotron Light (proposal number XAFS1–17750), Brazil.

References

[1] D.A. Reddy, C.L. Liu, R.P. Vijayalakshmi, B.K. Reddy, J. Alloy. Compd. 582 (2014) 257–264.
[2] X.S. Tang, E.S.G. Choo, L. Li, J. Ding, J.M. Xue, Chem. Mater. 22 (2010) 3383–3388.
[3] J. Cao, J. Yang, Y. Zhang, L. Yang, Y. Wang, M. Wei, Y. Liu, M. Gao, X. Liu, Z. Xie, J. Alloy. Compd. 486 (2009) 890–894.
[4] S. Ummartyotin, N. Bunnak, J. Juntaro, M. Sain, H. Manuspiya, Solid State Sci. 14 (2012) 299–304.
[5] G. Murugadoss, B. Rajamannan, V. Ramasamy, J. Lumin. 130 (2010) 2032–2039.
[6] R. Nasser, H. Elhouichet, M. Ferid, Appl. Surf. Sci. 351 (2015) 1122–1130.
[7] R. Viswanath, H.S.B. Naik, G.S.Y. Kumar, P.N.P. Kumar, G.A. Kumar, R. Praveen, J. Lumin. 153 (2014) 446–452.
[8] C. Corrado, Y. Jiang, F. Oba, M. Kozina, F. Bridges, J.Z. Zhang, JPCA 113 (2009) 3830–3839.
[9] V.A. Shuvaeva, I. Pirog, Y. Azuma, K. Yagi, K. Sakaue, H. Terauchi, I.P. Raevskii, K. Zhuchkov, M.Y. Antipin, J. Phys.-Condens. Matter 15 (2003) 2413–2421.
[10] V.A. Shuvaeva, D. Zekria, A.M. Glazer, Q. Jiang, S.M. Weber, P. Bhattacharya, P.A. Thomas, Phys. Rev. B 71 (2005) 174114.
[11] A. Michalowicz, J. Moscovici, D. Muller-Bouvet, K. Provost, J. Phys.: Conf. Ser. 190 (2009) 012034.
[12] A.L. Ankudinov, J.J. Rehr, J. Synchrotron Radiat. 10 (2003) 366–368.
[13] B.K. Agrawal, P.S. Yadav, S. Agrawal, Phys. Rev. B 50 (1994) 14881–14887.
[14] M.P. Klug, L.E. Alexander, X-Ray Diffraction Procedure for Polycrystalline and Amorphous Materials, Wiley-Interscience Publication, New York, 1974.
[15] M.M. Ferrer, Y.V.B. de Santana, C.W. Raubach, F.A. La Porta, A.F. Gouveia, E. Longo, J.R. Sambrano, J. Mol. Model. 20 (2014) 2375.
[16] S.S. Hasnain, Report on the International Workshops on Standards and Criteria in XAFS. in X-ray Absorption FineStructure: in: Proceedings of the VI International Conference on X-ray Absorption Fine Structures, Ellis Horwood New York.
[17] A.L. Curcio, M.I.B. Bernardi, A. Mesquita, Phys. Status Solidi C 12 (2015) 1367–1371.
[18] G.-C. Yi, Semiconductor Nanostructures for Optoelectronic Devices Processing, Characterization, and Applications, Springer, Heidelberg, Dordrecht, London, New York, 2012.
[19] B. Gilbert, B.H. Frazer, H. Zhang, F. Huang, J.F. Banfield, D. Haskel, J.C. Lang, G. Srajer, G. De Stasio, Phys. Rev. B 66 (2002) 245205.
[20] K. LawniczakJablonska, R.J. Iwanowski, Z. Golacki, A. Traverse, S. Pizzini, A. Fontaine, I. Winter, J. Hormes, Phys. Rev. B 53 (1996) 1119–1128.
[21] K. Lawniczakjablonska, R.J. Iwanowski, Z. Golacki, A. Traverse, S. Pizzini, A. Fontaine, Phys. B 208 (1995) 497–499.
[22] R. Kripal, A.K. Gupta, S.K. Mishra, R.K. Srivastava, A.C. Pandey, S.G. Prakash, Spectrochim. Acta Part a-Mol. Biomol. Spectrosc. 76 (2010) 523–530.
[23] S.J. Xu, S.J. Chua, B. Liu, L.M. Gan, C.H. Chew, G.Q. Xu, Appl. Phys. Lett. 73 (1998) 478–480.
[24] W.Q. Peng, G.W. Cong, S.C. Qu, Z.G. Wang, OptMa 29 (2006) 313–317.
[25] R.N. Bhargava, D. Gallagher, X. Hong, A. Nurmikko, Phys. Rev. Lett. 72 (1994) 416–419.